Journal of Alloys and Compounds 579 (2013) 227–235

Contents lists available at SciVerse ScienceDirect

Journal of Alloys and Compounds

journal homepage: www.elsevier.com/locate/jalcom

Luminescent properties of hybrid materials prepared by the polymeric precursor method

Larissa H. Oliveira [a,*], Ana Paula de Moura [a], Elson Longo [a], José A. Varela [a], Ieda L.V. Rosa [b]

[a] LIEC-UNESP, Institute of Chemistry, Caixa Postal 355, 14800-900 Araraquara, SP, Brazil
[b] LIEC-UFSCar, Department of Chemistry, Caixa Postal 676, 13560-905 São Carlos, SP, Brazil

ARTICLE INFO

Article history:
Received 12 April 2013
Received in revised form 4 June 2013
Accepted 9 June 2013
Available online 18 June 2013

Keywords:
Rare earth alloys and compounds
Chemical synthesis
Optical properties

ABSTRACT

Rare earth complexes (RE) can be incorporated in silica matrixes, originating organic/inorganic hybrid materials with good thermal stability and high rare earth emission lines. In this work, the hybrid material was obtained by the polymeric precursor method and ultrasonic dispersed with spherical silica particles prepared by the Stöber Method. The Raman spectra indicated that the Eu^{3+} ions are involved in a polymeric structure formed as consequence of the chelation and polyesterification reactions of this ion with citric acid and ethylene glycol. After the ultrasonic stirring, 2-hydroxynicotinic ligand will also compose this polymeric rigid structure. The TGA/DTA analysis showed that this polymeric material was thermal decomposed at 300 °C. Moreover, this process allows the chelating process of the 2-hydroxynicotinic acid ligand to the Eu^{3+} ions. The ^{29}Si NMR showed that the ultrasonic dispersion of the reactants was not able to promote the functionalization of the silica particles with the 2-hydroxynicotinic acid ligand. Moreover, heat treatment promotes the $[Eu(HnicO_2)_3]$ complex particles incorporation into silica pores. At this temperature, the TGA curve showed that only the thermal degradation of ethylene glycol and citric acid used during the experimental procedure occurs. The silica and hybrid materials are composed by spherical and aggregated particles with particle size of approximately 450 nm, which can be influenced by the heat treatment. These materials also present an absorption band located at 337 nm. The photoluminescent study showed that when the hybrid samples were excited at 337 nm wavelength, the ligand absorbs the excitation light. Part of this energy is transferred to the Eu^{3+} ion, which main emission, $^5D_0 \rightarrow {}^7F_2$, is observed in the emission spectrum at 612 nm. As the heating temperature increases to 300 °C, the energy transfer is more favorable. The lifetime values showed that the Eu^{3+} emission is enhanced due to the energy transfer process in the powders.

1. Introduction

The importance of rare earth elements is because of its particular luminescent properties, such as long lifetime and narrow emission lines. Thus, these elements can be employed in a broad range of applications, mainly including cathode ray tubes (CRTs), lasers and luminescent lamps [1]. On the other hand, the weak and narrow absorption bands of these lanthanides ions difficult its direct excitation process. In order to overcome this problem, the lanthanide ions, for example Eu^{3+} and Tb^{3+}, can be chelated with organic ligands. These molecules can also shield the metal ion from deleterious luminescence quenching interactions by O—H oscillators from solvent molecules [2]. The luminescence of these ions is obtained through the intramolecular energy transfer from excited state of the ligand to the emitting level of the lanthanide ion. This phenomenon is knowledge as "antenna effect" [3,4].

The factors such as poor stabilities under high temperature or moisture conditions and low mechanical strength limit their practical use. Thus, lanthanide complexes can be embedded into solid surfaces. When incorporated, its properties can be modified by interactions between the matrix and these organic complexes [5–7]. In this way, Langmuir–Blodgett films [8], porous glasses [9], oxide surfaces [10], and sol–gel glasses [11], has been applied as hosts to embedded many lanthanide ions. Among them, silica is one of the most inorganic substances used as support for several systems due to its easiness to control size and shape of particles, and also to control volume and pore size distribution as well as surface area, when compared to other metals such as titanium, zirconium or aluminum [12].

The sol–gel technique can be a suitable wet chemical route to synthesize lanthanide silica-based organic/inorganic hybrid material due to mild synthetic condition and processing versatile. The incorporation of lanthanide complexes into silica gel matrix, which

* Corresponding author. Address: LIEC-UNESP-Instituto de Química, Rua Francisco Degni, 55, CP 676 CEP 14800-900, Araraquara, SP, Brazil. Tel.: +55 16 33519828x9894.
E-mail address: larissahelena2009@gmail.com (L.H. Oliveira).

0925-8388/$ - see front matter © 2013 Elsevier B.V. All rights reserved.
http://dx.doi.org/10.1016/j.jallcom.2013.06.051

is based on hydrolysis and polycondensation reactions, give rise to multifunctional materials allowing the formation of direct chemical bonds between the organic and inorganic components and, furthermore, it is possible to tune its optical properties [13–15].

However, there are some drawbacks like low stability and solubility of the complexes at the low pH needed for the hydrolysis reaction, the cracking of the materials during the drying period and the presence of water molecule in the silica pores. Thus, polymers molecules can be introduced into these materials to solve this problem. Generally, the most used polymers containing carbonyl groups are Polyvinyl butyral (PVB), Polyvinylpyrrolidone (PVP) and Polymethylmethacrylate (PMMA). Firstly, these groups are grafted onto silica microsphere by means of Si—O bonds, then, the lanthanide complexes are introduced above the system polymer-SiO_2 through their coordination reaction resulting in a rigid hybrid system [16–18].

Based on the papers published in the last years, the polymeric precursor method has been chose to synthesized hybrid materials, in this study. These investigations were encouraged by the possibility to control the homogeneity of the systems in molecular level as well as the production of particles with uniform size in a reactional procedure at low temperature. Moreover, using this methodology, the organic reagents used during the synthesis can be decomposed by the thermal treatment used. Besides that, hybrid materials can be synthesized in a shorter period of time (~2 h) when compared to other systems like EDTA-Ln-TTA-SiO_2 where Ln = Eu, Tb and Gd [19].

The silica-based hybrid materials can be classified according to its composition, nature of interactions or chemical bonds involved: The Class I hybrid material concerns the conventional doping systems in which only weak interactions, such as hydrogen bonding, van der Waals forces and/or weak static effects, exists between the organic and inorganic components. In the Class II hybrid material, the organic and inorganic components are covalently linked [20,21]. Recently, several organic ligands have been used in the obtention of silica-based hybrid materials, such as terpyridine [22], 1,10-fenantroline [23], bypyridine [3] and dicarboxilic acids [24,25]. The heretocyclic 2-hydroxynicotinic acid ligand, shown in Fig. 1, is a heterocyclic ligand which has been widely used for synthesizing transition metal ion complexes [26–28]. This organic ligand exhibit enol–keto tautomerism transformation in the solid state and in solution, due to the mobility of the unstable hydrogen atom of the OH group, giving rise to different coordination modes of $HnicO^-$ including monodentade, bridging, N,O-chelating, and O,O-chelating that could result in a large diversity of coordination compounds, as described elsewhere [29].

The luminescent properties of these materials showed that an intramolecular energy transfer from the organic ligand to RE ions is involved, and also shows the promising applications that these classes of materials are therefore expected in nano-technological fields. Thus, in this present paper, a lanthanide silica based organic/inorganic hybrid material was prepared by the polymeric precursor method [30], where the spherical silica particles was employed as host inorganic matrix, and the lanthanide complex formed between the heterocyclic ligand 2-hydroxynicotinic acid (H_2nicO) and Eu^{3+} ion composed the organic component. These hybrid materials were characterized by Fourier transform Raman spectroscopy (FT-Raman), thermal analysis (TGA/DTA), field emission scanning electron microscopy (FE-SEM), ^{29}Si Nuclear magnetic ressonance spectroscopy (^{29}Si NMR). The photophysical properties were investigated through the Uv–vis absorbance spectroscopy and by the excitation and emission spectra of the Eu^{3+} ion as well as its lifetime in ms.

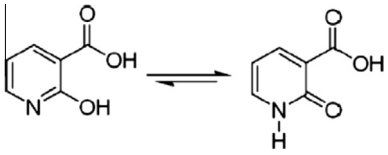

Fig. 1. Molecular structure and enol-ketone tautomeric mechanism of the 2-hydroxynicotinic (H_2nicO) ligand [20].

2. Experimental section

2.1. Synthesis of the spherical silica particles

The Stöber Method [31] was employed in the synthesis of the spherical silica particles, which is based on the hydrolysis of the TEOS catalyzed by the ammonia. An amount of ethanol and TEOS was stirred for some minutes. To this solution were quickly added ethanol, ammonia and deionized water. The recipient was hermetically closed and stayed under stirring for more 4 h. After that, the solvent was evaporated and the solid obtained was dried in a furnace at 100 °C for 12 h, where it was obtained 2.54 g of spherical silica.

2.2. Synthesis of the hybrid materials

The resin used for synthesize the hybrid materials was prepared by the polymeric precursor method [32] using an aqueous Eu^{3+} citrate solution prepared from europium nitrate (europium oxide in nitric acid) and citric acid. The citric acid/Eu^{3+} ratio was fixed at 3:1 (mol%). Ethylene glycol was added to the citric acid solution using a mass ratio (citric acid/ethyleneglycol) of 40:60. The Eu^{3+} complex organic phase onto the spherical SiO_2 surface was prepared by a wet and soft chemical method [33]. An amount of 1.0 g of spherical SiO_2 was added in 25 mL of deionized water and then sonicated for 5 min. An aqueous solution containing the 2-hydroxynicotinic acid ligand (pH 6.0) was also prepared. The resin containing Eu^{3+} ions was mixed to the aqueous solution with the organic ligand. Afterwards, the solution was dispersed on the spherical SiO_2 aqueous solution and then sonicated for 5 min. The solvent was evaporated to obtain the SiO_2-[Eu(HnicO)] sample, and then was dried at 100 °C for 12 h resulting the Hybrid I and 300 °C for 2 h giving rise to Hybrid II using a heating rate of 5 °C/min.

2.3. Synthesis of the lanthanide complex

Firstly, a $Eu(NO_3)_2{\cdot}nH_2O$ solution was prepared by dissolving 0.01 mol of Eu_2O_3 in HNO_3 under stirring. The lanthanide complex were prepared by adding aqueous solution (5 mL) of the respective lanthanide salt ($Eu(NO_3)_2{\cdot}nH_2O$) to an aqueous solution (15 mL, pH 6.0) of 2-hydroxynicotinic acid. The ligand quantity added to the lanthanide salt solution was measured using a RE ion/ligand ratio of 1:3 mol. After stirring the mixture for same minutes a white powder started to precipitate in the beaker. The powder was filtered and dried at 100 °C for 12 h. This experimental procedure is in accordance to describe in Ref. [34].

2.4. Characterization

The powder morphologies were verified using a scanning electron microscope (Jeol JSM-7500F microscope). Fourrier transform Raman data were obtained at room temperature using a RFS/100/S Bruker FT-Raman equipment with spectral resolution of 4 cm^{-1} attached to a Nd:YAG laser, promoting an excitation light of 1.064 nm in the frequency range of 500 up to 3500 cm^{-1}. The ^{29}Si NMR spectra were collected in a VARIAN Unity 400 spectrophotometer operating in 79.5 MHz with a high efficient decoupling using a scanning in the room temperature. For acquisition of the ^{29}Si NMR spectra was used a zirconium oxide rotor of 7 mm diameter and 6 kHz speed and the magic angle speed technique (MAS) with a recycle of 0.3 s between 90° pulses was also performed. The thermal analysis was recorded in Netzsch-Thermische Analyse STA 409 cell equipment using a heating rate of 5 °C/min and synthetic air atmosphere. Ultraviolet visible absorption spectra of the as-prepared materials were performed using Cary 5G equipment. The emission and excitation spectra of these samples were obtained under a 450 W xenon lamp source in a JOBIN YVON SPEX TRIAX 550-FLUOROLOG III spectrofluorometer at room temperature. Lifetime data of the Eu^{3+} $^5D_0 \rightarrow {}^7F_2$ transition of the [$Eu(HnicO_2)_3$] complex, Hybrid I and Hybrid II powders were evaluated from the decay curves using the emission wavelength set at 613 nm and excitation wavelength set at 393 and 337 nm.

3. Results and discussion

3.1. Fourrier transform Raman (FT-Raman)

Fig. 2 presents the FT-Raman spectra of the free ligand (a), [$Eu(HnicO_2)_3$] complex (b) Hybrid I (c) and Hybrid II (d) powders.

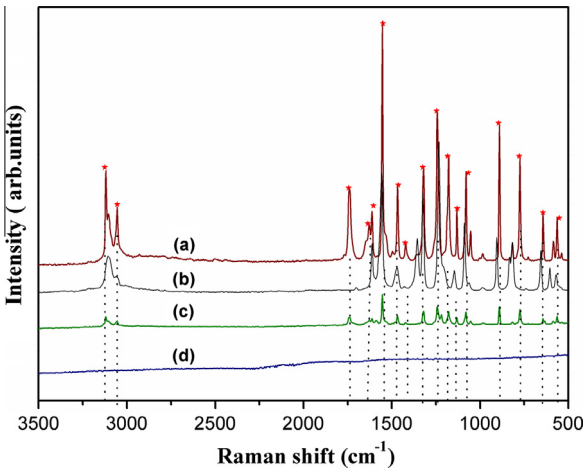

Fig. 2. FT-Raman spectra of the 2-hydroxynicotinic acid free ligand (a), [Eu(HnicO_2)$_3$] complex (b) Hybrid I (c) and Hybrid II (d).

From the Raman spectrum of the free ligand (Fig. 2a), the presence of some active modes at 3125 and 3063 cm^{-1} ascribed to the ν(N—H) and ν(O—H) vibrational modes were detected. The peak referring to the stretching mode of C=O linkage appears at 1744 cm^{-1}, as well as the C—O deformation vibration modes at 1185 and 1175 cm^{-1}, respectively. The Raman peak ascribed to the asymmetric stretching mode also appears at 1635 cm^{-1}. It was also observed some Raman modes at 1322 and 1175 cm^{-1} referring to the symmetric stretching vibration of the CO_2^- bonds. The Raman peak at 1549 cm^{-1} was attributed to the ν(CC) and the $\nu(CO_2)$ was noted at 1463 and 1424 cm^{-1} as well as the $\delta(CO_2)$ in-plane at 647 cm^{-1}. The deformation vibration mode of the OH groups appears at 894 cm^{-1}. The Raman modes ascribed to the δ(NH) in the plane and out of the plane were observed at 1604 and 551 cm^{-1}, respectively. Finally, the deformation vibration modes of the C—C—O bonds appear at 450 cm^{-1}. The Raman peak positions are listed at Fig. 2a–c and Table 1, respectively.

The obtained results in Fig. 2b for the [Eu(HnicO_2)$_3$] complex showed Raman vibration modes at 3102, 3063, 1612, 1557, 1463, 1320, 1235, 1100, 900, 817, 655 and 559 cm^{-1}. However, this spectrum presented some differences when compared to the free ligand (Fig. 2a and b). The first difference can be noted by a shift in the Raman vibrational modes at 1635 cm^{-1}. The second one is related to the disappearance of the Raman modes at 1744, 1424, and 1604 cm^{-1} ascribed to the ν(C=O), $\nu_s(CO_2)$, and δ(NH) in the plane mode, respectively. Moreover, the changes observed on the characteristic positions of Raman peaks (Table 1) can be possibly related to the chelating of the 2-hydroxynicotinic ligand with Eu^{3+} ions via O,O-coordination, as shown in Fig. 3a.

Table 1
Raman vibrational modes peak position observed in the FT-Raman spectra of the free ligand, [Eu(HnicO_2)$_3$] complex, Hybrid I and Hybrid II powders prepared by polymeric precursor method.

Attribution	Powders			
	2-Hydroxynicotinic acid ligand	[Eu(HnicO_2)$_3$]	Hybrid I	Hybrid II
ν(N—H)	3125	3102	3116	–
ν(O—H)	3054	3063	3054	–
ν(C=O)	1744	–	1742	–
$\nu_{as}(CO_2)$	1635	1612	1620	–
ν(CC)	1549	1557	1548	–
$\nu_s(CO_2)$	1473/1424	1463	1469	–
$\nu_s(CO_2^-)$	1322/1243	1320/1235	1325/1237	–
ν(C—O)	1185/1175	1100	1176	–
Rocking CH_3 vibration	–	–	1132/1086	–
ν_{as}(COC)	–	–	890/770	–
ν(OH)	894	900/817		–
$\delta(CO_2)$ in plane	647	655	647	–
δ(NH) in the plane/ out of the plane	1604, 551	559	562	–
ν(CCO)	450	–	456	–

The Raman spectrum of Hybrid I powder (Fig. 2c) presented the same feature of the [Eu(HnicO_2)$_3$] complex, however, two more Raman modes appear in its Raman spectrum. One Raman mode appears at 1132 and 1086 cm^{-1}, which are ascribed to the rocking CH_3 vibration mode and the second one appears at 890 and 770 cm^{-1} and is related to the asymmetric vibration mode of the C—O—C bonds. Both modes appear in recurrence of polymeric skeleton involving the Eu^{3+} ions.

As described in Section 2, the polymeric precursor method is based on the preparation of a polymeric resin, which is obtained by means of a chelating or complexation process of the metallic ions (Eu^{3+} ions) with the citric acid (Fig. 3b) followed by its polymerization, using a polymeric agent like ethylene glycol. In this last process, a polyestherification reaction occurs, resulting in a dimer as illustrated at Fig. 3c. At the end of this process, it was obtained a polyester molecule where Eu^{3+} ions are located and are homogeneously dispersed in the polymeric structure (Fig. 3c).

When the 2-hydroxyniconitic acid solution at pH = 6.0 was added, the carboxyls groups from the ligands linked to the hydroxyls groups from the polymeric skeleton around the Eu^{3+} ions through weak interactions, such as hydrogen bonding, van der Waals forces and/or weak static forces, giving rise to a rigid polymeric matrix (Fig. 3c) [32,33].

From all published papers about hybrid materials in the literature, we highlight of Li et al. [3], which also used the 2-hydroxynicotinic acid ligand to synthesized hybrid materials by the sol–gel method. In this paper, the 3-(triethoxysyl)-propyl-isocianate (TESPIC) was used to assembling the RE ions as well as the 2-hydroxynicotinic acid in a silica based inorganic matrix by means of ester linkages (covalent linkages). The grafting of these groups to the silica matrix has been made during the hydrolysis and polycondensation processes.

Comparing this hybrid material with the silica based organic–inorganic hybrid material prepared by the polymeric precursor method it is possible to say that the polymeric matrix formed by citric acid and ethylene glycol was synthesized separately from the silica Stöber. After that, the incorporation of this polymeric structure into the SiO_2 structure occurs during the ultrasonic dispersion process. All these steps facilitates the thermal decomposition of citric acid and ethylene glycol at lower temperatures (<500 °C), and allows the chelating process of the 2-hydroxynicotinic acid ligand to the Eu^{3+} ions.

In the Raman spectra of the Hybrid II powder (Fig. 2d) the vibrational modes related to the 2-hydroxynicotinc acid are too weak to be detected. All results are in accordance with Refs. [34–36].

3.2. ^{29}Si Nuclear magnetic resonance spectroscopy (^{29}Si NMR)

^{29}Si NMR spectroscopy in the solid state is an important tool for the characterization of hybrid inorganic/organic silica based materials, because it is able to differentiate the Si atoms in its structure according to their neighbors and, besides that, contributes significantly in the comprehension of the organic groups distribution, as well as the identification of Si atoms bounded to carbon atoms. Fig. 4 presents ^{29}Si NMR spectra of the SiO_2, Hybrid I and Hybrid II powders, respectively. In the case the spherical silica spectrum three signals (Q^4, Q^3 and Q^2) were detected, which are related to the presence of silanols and siloxanes groups in the silica surface (Q^n), where n = 4, 3, 2, represents the siloxanes groups linked to the Si atoms. These signals are related to the siloxanes (silicon atoms bounded

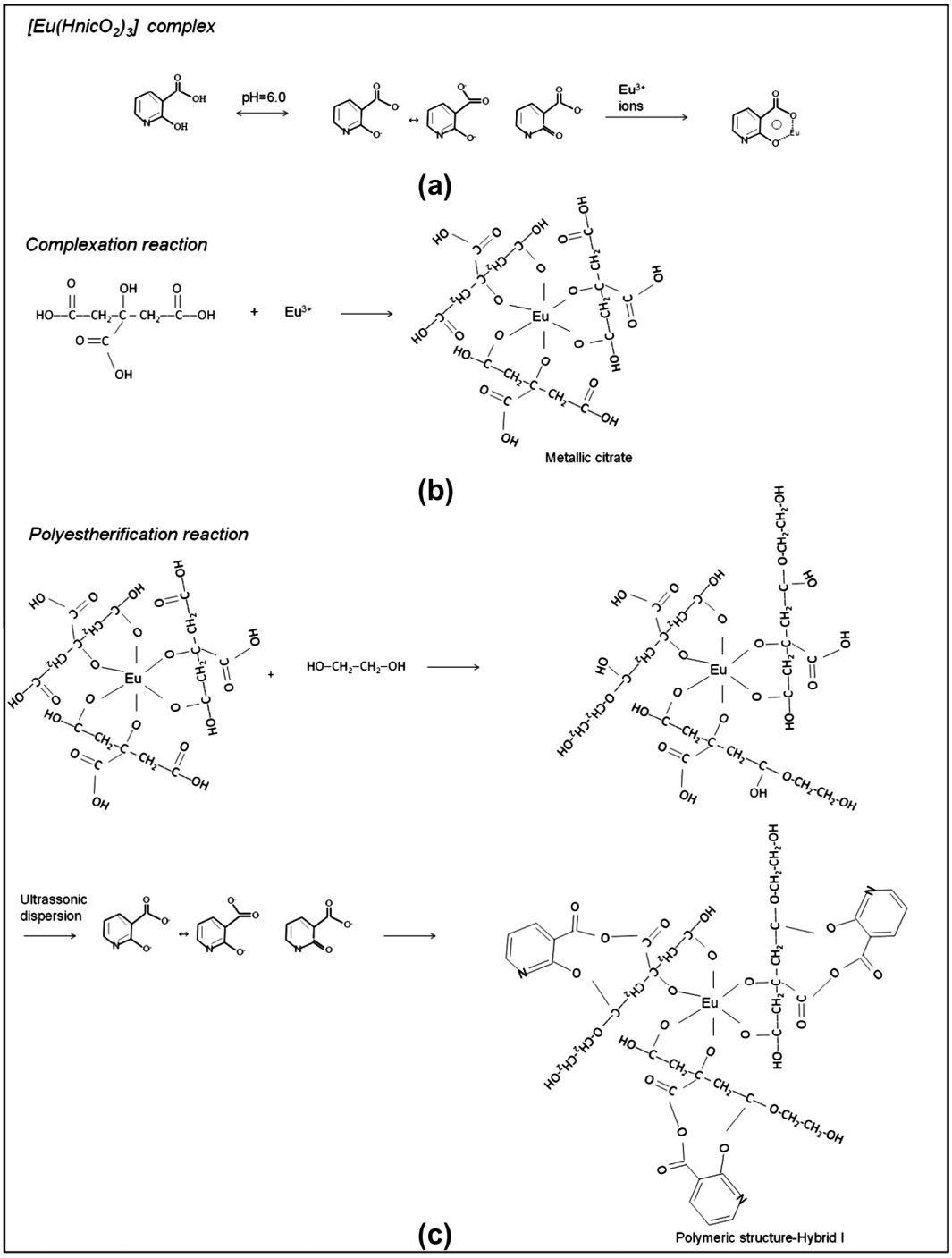

Fig. 3. (a) O,O-coordination for the 2-hydroxynicotinic acid ligand in the obtained complex: π-electron resonance between the oxygen atoms, (b) complexation reaction of the Eu^{3+} ions with citric acid in the polymeric precursor method and (c) polyestherification reaction and 2-hydroxynicotinic acid grafting to the polymeric resin.

to four oxygen atoms), to the silanols groups [$(SiO_3)SiOH$)] and to the geminals silanols groups [$Si(OSi)_2(OH)_2$] (Fig. 4). And also these signals appear at −110 ppm, −101 ppm and −92 ppm, respectively [37–39]. These three signals were also detected for Hybrid I powder, indicating the ultrasonic dispersion of the reactants was not able to promote the functionalization of the silica particles with the polymeric structure. However, for Hybrid II powder, a decrease in the intensity of the Q^2 and Q^3 groups, indicating the formation of silane linkage in the silica surface, due to the water loss at silica surface as the heat treatment increases from 100 to 300 °C. Moreover, the NMR spectrum (Fig. 4) also indicates that the hybrid organic–inorganic particles are into silica pores.

3.3. Thermogravimetic analyses (TGA/DTA)

Fig. 5 presents the TGA curve of the 2-hydroxyniconic acid ligand (a) [$Eu(HnicO_2)_3$] complex (b) and Hybrid I (c) samples.

The TGA curve in Fig. 5a showed that in the temperature ranges from 50 to 291 °C the thermal degradation of the 2-hydroxynicotinic acid occurs. However, for the [$Eu(HnicO_2)_3$] complex, 35% of its thermal degradation only occurs at approximately 550 °C. In the Hybrid I material (Fig. 5b), a weight loss of 30% occurs at the same temperature range, as observed for the free ligand. From these results, we deduced that the thermal treatment at 300 °C was able to eliminate the ethylene glycol and citric acid, of the

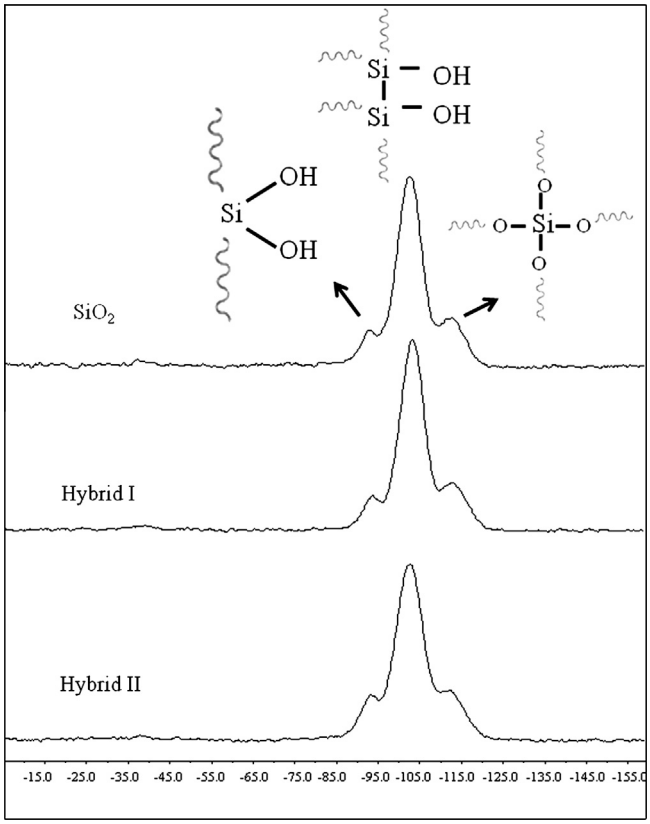

Fig. 4. ^{29}Si NMR spectra of SiO_2, Hybrid I and Hybrid II powders, respectively.

polymeric structure around the Eu^{3+} ions. Besides that, the lower height loss also indicates that the 2-hydroxynicotinic acid organic ligand still remains in the Hybrid II material. At higher temperatures both materials became more stable and none weight loss was observed. The thermal treatment promotes structural rearrangements in these materials. These changes were analyzed by the spectroscopic properties of the Eu^{3+} ion through the study of the emission and excitation spectra of Eu^{3+} in the materials.

3.4. Field-emission scanning electron microscopy (FE-SEM)

The morphological study of the hybrid inorganic/organic materials synthesized by the polymeric precursor method [23] was performed through the FE-SEM analysis. Fig. 6 presents the micrographies of the spherical Stöber silica (a), Hybrid I (b) and Hybrid II(c), and the histograms for silica (d), Hybrid I (e) and Hybrid II (d), respectively.

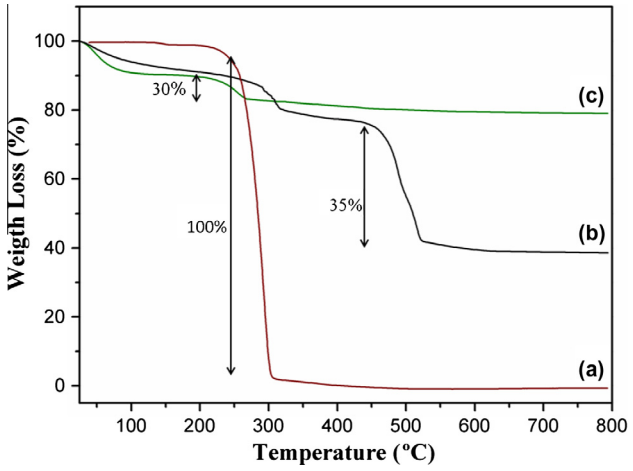

Fig. 5. Thermogravimetric curve of the 2-hydroxynicotinic acid ligand (a), $[Eu(HnicO_2)_3]$ complex (b) and Hybrid I (c) 6 powders.

The spherical Stöber silica image in Fig. 6a, presented spherical and monodispersed particles. This morphology remains the same after the heat treatment, and also some irregular particles between them were detected, which is probably composed by polymeric structure. In this case, we suppose that a Class I silica-based hybrid material is formed. This material is composed by silica spherical particles and polymeric structure linked through van der Waals forces in its surface.

However, when this material was treated at 300 °C, the irregular particles disappeared. In this process the thermal decomposition of citric acid and ethylene glycol occurs, giving rise to the $[Eu(HnicO_2)_3]$ complex species which are probably into the silica pores, since in this temperature was no thermal decomposition (Fig. 5). Thus, we supposed that the heat treatment promoted the formation of a Class II hybrid material. All these results are in agreement with ^{29}Si NMR and TGA analyses.

Although the pure silica particles presented a spherical shape, their size varied from a few nanometers. Thus, a histogram with the average size of these particles was measured using the Image J program and the results are listed in Fig. 6d–f. From the obtained results it was observed that the spherical silica particles (Fig. 6d) presented a narrow dispersion of the average size. After the introduction of the $[Eu(HnicO_2)_3]$ complex, the as-prepared Hybrid I material (Fig. 6e) presents spherical silica particles with a large dispersion of average size and almost of these particles in both systems presents a size of 490 nm. As the temperature increases for 300 °C, the particles become smaller and presented a particle size of around 430 nm, as a consequence of the thermal degradation of the organic material (ethylene glycol and citric acid) used in the experimental procedure.

3.5. UV–vis absorption spectroscopy

Fig. 7 presents the UV–vis absorbance spectra of the spherical silica (a) 2-hydroxynicotinic acid ligand (b), $[Eu(HnicO_2)_3]$ complex (c), Hybrid I (d) and Hybrid II (e) powders.

From these spectra it was observed that the spherical silica particle presents a little intense broad absorption band in the range of 200–250 nm (♠) with a maximum situated at approximately 220 nm (Fig. 7a). For 2-hydroxynicitonic acid free ligand (Fig. 7b) a broad band with a maximum at 337 nm (♦) was observed, ascribed to the major π–π^* electronic transitions. This broad band can be also noticed in the absorption spectrum of the $[Eu(HnicO_2)_3]$ complex, Hybrid I and Hybrid II powders in Fig. 7c–e, respectively. However, for Hybrid II powder the broad band was shifted to 307 nm due to the conjugating effect of double bonds and enlargement of the energetic levels among the electron transitions [16], caused by the coordination of the 2-hydroxynicotinic acid with Eu^{3+} ions and its incorporation to the spherical silica. The other absorption bands observed at Fig. 7c, of the $[Eu(HnicO_2)_3]$ complex are ascribed to the Eu^{3+} $4f^6$ electronic transitions, which are absent in the Hybrid I and Hybrid II powders absorbance spectra (Fig. 7d–e), since it was overlapped by the broad band of the silica matrix.

3.6. Luminescent properties

Fig. 8 presents the excitation spectra of the $[Eu(HnicO_2)_3]$ complex (a) Hybrid I (b) and Hybrid II (c) having the emission set at 613 nm. The powders show the presence of a broad band with a maximum situated at 337 nm, attributed mainly to the ligand-metal charge transfer band (LMCT) from the 2-hydroxynicotinic acid

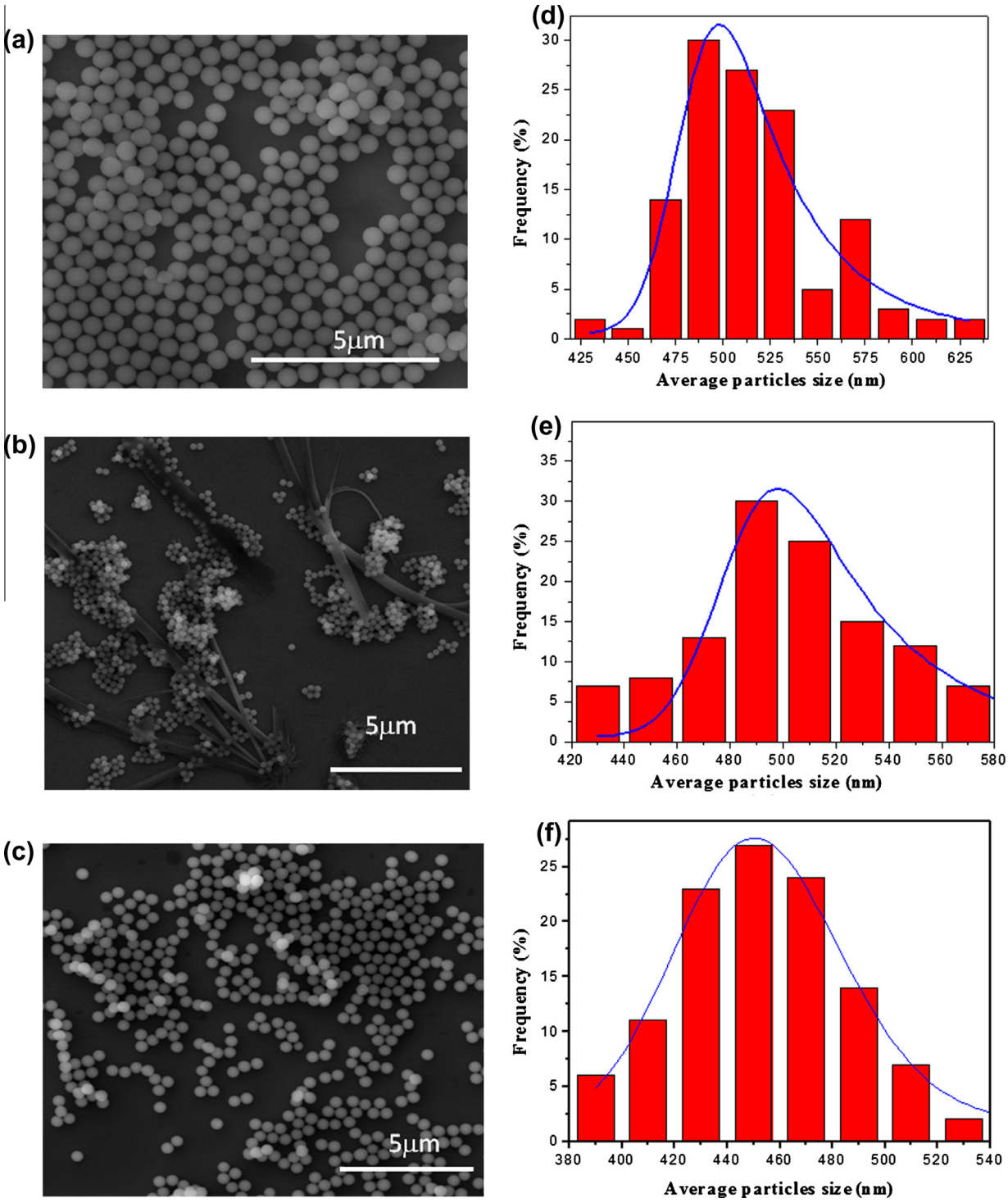

Fig. 6. FE-SEM images of the spherical silica Stöber particles (a), Hybrid I (b), Hybrid II (c) powders, and the histograms for silica (d), Hybrid I (e) and Hybrid II (d), respectively.

to the Eu^{3+} ion. This effect can also be caused by the polymeric environment around the Eu^{3+}, where, besides the 2-hydroxynicotinic acid ligand, it is also present the citric acid and the ethylene glycol used in the synthesis process. For $Eu(HnicO_2)_3]$ complex (Fig. 8a) it was observed the broad band from the ligand and the $4f^6$ intra-configurational characteristic transition bands (●) of the Eu^{3+} ion. They are ascribed to the electronic transitions from the ground state $^7F_0$ to the following excited states: $^5H_4$ at 391 nm, $^5L_6$ at 392 nm, $^5D_2$ at 465 nm and $^5D_1$ at 536 nm [40].

For the Hybrid I powder (Fig. 8b), besides the broad band at 337 nm, it was noticed the $^7F_0 \rightarrow {}^5L_6$ Eu^{3+} excitation band at 392 nm and the $^7F_0 \rightarrow {}^5D_2$ Eu^{3+} excitation band at 462 nm, confirming the formation of a class I hybrid material, where both organic and inorganic phases behave independently. In the excitation spectra of the Hybrid II powder (Fig. 8c), we did not indentified the characteristic $4f^6$ intra-configurational transitions of the Eu^{3+} ion, due to the incorporation of $[Eu(HnicO_2)_3]$ complex by the silica pores. The organic ligand excitation broad band overlaps the Eu^{3+}

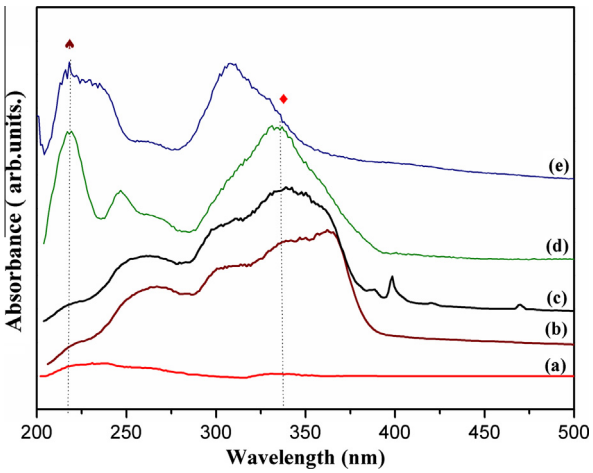

Fig. 7. UV–vis spectra of the spherical silica (a) 2-hydroxynicotinic acid ligand (b), $[Eu(HnicO_2)_3]$ complex (c), Hybrid I (d) and Hybrid II (e) powders.

one, so in this material the Eu^{3+} ions are excitated via energy transfer from the 2-hydroxynicotinic acid supported in the SiO_2 matrix. In this material the organic ligands promotes an excellent antenna effect since the Eu^{3+} emission intensity is enhanced in almost nine times when excited at around 337 nm. Another interesting feature observed was that these powders can also be excited in a wide range covering from UV (~280 nm) to near UV (~350 nm) spectra.

When the Eu^{3+} ion is incorporated to inorganic systems, it is excitated by an irradiation light at 394 nm, ascribed to the $^7F_0 \rightarrow {}^5L_6$ level. The electronic transitions observed in the emission spectrum refers to a radiative decay from $^5D_0$ to ^7F_J (J = 0, 1, 2, 3, 4, 5, 6) levels of the $4f^6$ configuration of this ion. They also appear in the red region of the electromagnetic spectrum [41–44].

As it can seen in Fig. 9A, the emission spectra of the $[Eu(HnicO_2)_3]$ complex (λ_{em} = 613 nm), presents the bands at 578, 582, 612, 649 and 698 nm, characteristics of the Eu^{3+} $^5D_0 \rightarrow {}^7F_J$ (J = 0, 1, 2, 3 and 4) transitions, respectively. The same bands at the emission spectra of the Hybrid I and Hybrid II powder were detected (Fig. 9B). In these emission spectra the most intense band is ascribed to the $^5D_0 \rightarrow {}^7F_2$ transition at 613 nm. The electronic transition in the Hybrid I and II spectra is broader and less outspreading than the $[Eu(HnicO_2)_3]$ complex, as a consequence of the incorporation of the organic material by the silica matrix. In the Hybrid I material the polymeric structure containing the Eu^{3+} and the 2-hydroxynicotinic acid ligand are between the silica particles, unlike, the Hybrid II presents the $[Eu(HnicO_2)_3]$ complex species in its pores. In this case, the energy transfer becomes more favorable, due to the formation of a Class II silica-based hybrid material.

The decay curves of the Eu^{3+} $^5D_0 \rightarrow {}^7F_2$ transition for the $[Eu(HnicO_2)_3]$ complex, Hybrid I and Hybrid II powders (not shown), presented a mono-exponential feature when this ion was excited in both excitation wavelengths of 394 and 337 nm (λ_{em} = 613 nm).

According to literature publication [45], the lifetime (τ), non-radiative (A_{nRad}) and radiative (A_{Rad}) rates are related through the following equation: $A_{tot} = 1/=A_{Rad} + A_{nRad}$, where the A_{Rad} rate was obtained by summing over the radiative rates A_{0J} for each $^5D_0 \rightarrow {}^7F_J$ transition is given by $A_{Rad} = \sum_J A_{0J}$. The emission quantum efficiency of the emitting $^5D_0$ level is given by:

$$\eta = \frac{A_{Rad}}{A_{Rad} + A_{nRad}}$$

The Eu^{3+} lifetime values in Table 2, presented an increase when the excitation was made in 337 nm, compared to the 394 nm one. For the $[Eu(HnicO_2)_3]$ complex excited at 337 nm the emission process is enhanced due to the energy transfer from the 2-hydroxynicotinic anion to the Eu^{3+} ions.

Quantum efficiencies for $[Eu(HnicO_2)_3]$ complex, Hybrid I and Hybrid II samples at 337 nm were evaluated as 30%, 31% and 26%, respectively. At this excitation wavelength, the Hybrid I powder presented a higher quantum efficiency, which is consistent with a higher lifetime (0.45 ms) due to the higher interaction

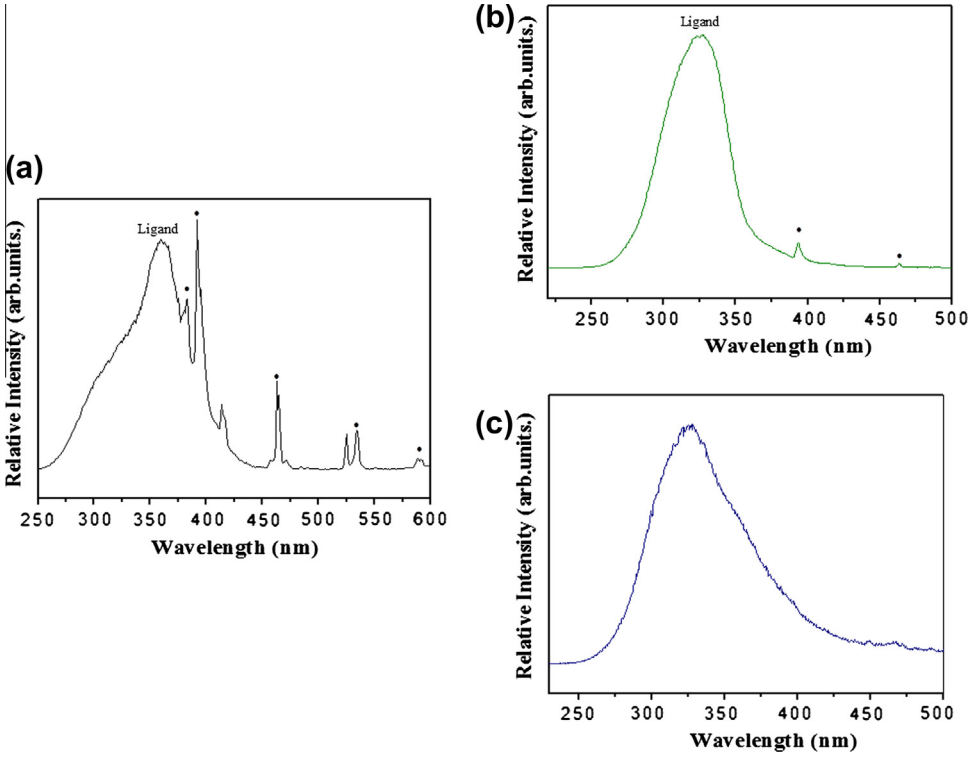

Fig. 8. Excitation spectra of the $[Eu(HnicO_2)_3]$ complex (a) Hybrid I (b) and Hybrid II (b), λ_{em} = 613 nm.

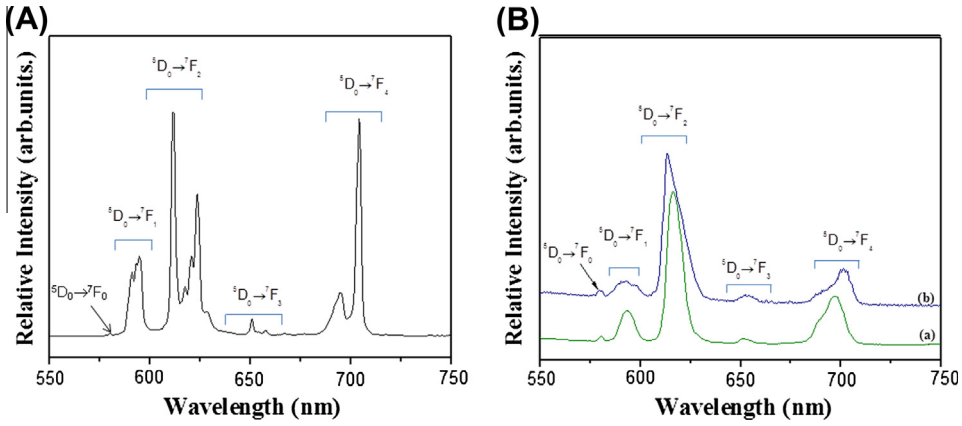

Fig. 9. Emission spectra of the (A) $[Eu(HnicO_2)_3]$ complex and (B) Hybrid I (a) and Hybrid II (b), $\lambda_{exc.}$ = 337 nm.

Table 2
Emission quantum efficiencies (η), lifetime (τ), non-radiative (A_{nRad}), and radiative (A_{Rad}) for the $[Eu(HnicO_2)_3]$, Hybrid I and Hybrid II powders.

Samples	τ/ms 394 nm	τ/ms 337 nm	A_{Rad} (s^{-1})	A_{nRad} (394) (s^{-1})	A_{nRad} (337) (s^{-1})	η(394) (%)	η(337) (%)
$[Eu(HnicO_2)_3]$	0.42	0.43	207.56	494	482	29.6	30
Hybrid I	0.36	0.45	207.15	573	460	26.5	31.0
Hybrid II	0.30	0.35	183.34	611	523	23.0	26.0

between the Eu^{3+} ion and the polymeric material, composed by 2-hydrixynicotinic ligand, citric acid and ethylene glycol, in a way to form a hybrid complex structure. This effect can be interpreted as a decrease in the non-radiative combination centers of the Eu^{3+} ions, which contributes to the multiphonon deactivation at the $^5D_0$ level. This level is almost depopulated which lowers the rate of vibronic coupling and results in an increase in the Eu^{3+} emission luminescence lifetime [46]. On the other hand, Hybrid II sample treated at 300 °C presents a lifetime of 0.35 ms. This value indicates the presence of a huge quantity of silanols groups around the Eu^{3+} ion, as a consequence of the incorporation of the $[Eu(HnicO_2)_3]$ complex into the silica pores. Thus, a higher non-radiatives energy losses occurs (A_{nRad} = 523 s^{-1}).

In this work, the quantum efficiencies values calculated for the silica based organic–inorganic hybrid materials prepared by the polymeric precursor method is not so different from the literature data for sol–gel method, which presents quantum efficiencies in range of 13.8% and 34.09%, depending on the used polymer [2,19].

4. Conclusion

In summary, silica based hybrid materials were synthesized by the polymeric precursor method. The Raman spectra indicated that the Eu^{3+} ions are involved in a polymeric structure formed as a consequence of the chelation and polyesterification reactions of this ion with citric acid and ethelyne glycol. After the ultrasonic stirring, 2-hydroxynicotinic ligand will also compose this polymeric rigid structure. The TGA/DTA analysis showed that this polymeric material was thermal decomposed at 300 °C. Moreover, this process allows the chelating process of 2-hydroxynicotinic acid ligand with Eu^{3+} ions. The ^{29}Si NMR and FE-SEM analysis showed that the ultrasonic dispersion of the reactants was not able to promote the functionalization of the silica particles with the 2-hydroxynicotinic acid ligand and a Class I hybrid material was detected. However, as the thermal treatment increases to 300 °C is proposed that $[Eu(HnicO_2)_3]$ complex is probably into the silica pores, and a Class II hybrid material was formed. The silica and hybrid materials were composed by spherical and aggregated particles with particle size of approximately 450 nm, which can be influenced by the thermal degradation of ethylene glycol and citric acid used in the experimental procedure. The photoluminescent study showed that when the hybrid samples were excited at 337 nm, the ligand absorbs the excitation light. Part of this energy is transferred to the Eu^{3+} ion, which main emission, $^5D_0 \rightarrow ^7F_2$, is observed in the emission spectrum at 613 nm. As the heating temperature increases for 300 °C, the energy transfer is more favorable. The lifetime values showed that the Eu^{3+} emission is enhanced due to the energy transfer process between the ligands and the luminescent ion.

Acknowledgments

The authors acknowledge the financial support of the Brazilian research financing institutions: CNPq, CAPES and FAPESP. Special thanks for Prof. Dr. Oswaldo A. Serra for the luminescence measurements.

References

[1] S. Gago, J.A. Fernandes, J.P. Rainho, R.A.S. Ferreira, M. Pillinger, A.A. Valente, T.M. Santos, L.D. Carlos, P.J.A. Ribeiro-Claro, I.S. Gonçalves, Chem. Mater. 17 (2005) 5077–5084.
[2] J. Xu, Y. Ma, L. Jia, X. Huang, Z. Deng, H. Wang, W. Liu, Y. Tang, Mater. Chem. Phys. 133 (2012) 78–86.
[3] H. Li, J. Yu, F. Liu, H. Zhang, L. Fu, Q. Meng, C. Peng, J. Lin, New J. Chem. 28 (2004) 1137–1141.
[4] Q.M. Wang, B. Yan, J. Organomet. Chem. 691 (2006) 3567–3573.
[5] E. De Oliveira, C.R. Neri, O.A. Serra, A.G.S. Prado, Chem. Mater. 19 (2007) 5437–5442.
[6] C.P. McCoy, F. Stomeo, S.E. Plush, T. Gunnlaugsson, Chem. Mater. 18 (2006) 4336.
[7] Q. Li, T. Li, J.G. Wu, J. Phys. Chem. B 105 (2001) 12293.
[8] O.A. Serra, I.L.V. Rosa, C.L. Medeiros, M.E.D. Zanquelli, J. Luminesc. 60 (1994) 112.
[9] D. Avnir, D. Levy, R. Reisfeld, J. Phys. Chem. 88 (1984) 5956.
[10] J. Zhang, G. Gao, D. Zhang, C. Wang, D. Zhao, F. Liu, J. Colloid Interface Sci. 301 (2006) 78.
[11] L.R. Matthews, E.T. Knobbe, Chem. Mater. 5 (1993) 1697.
[12] E.V. Benvenutti, C.C. Moro, T.M.H. Costa, M.R. Gallas, Química Nova 32 (7) (2009) 1926–1933.
[13] J. Xu, L. Jia, Y. Ma, X. Liu, H. Tian, W. Liu, Y. Tang, Mater. Chem. Phys. 136 (2012) 112–119.

[14] F.F. Wang, B. Yan, J. Fluoresc. 17 (2007) 418–426.
[15] L.D. Carlos, R.A.S. Ferreira, V.Z. Bernudez, S.J.L. Ribeiro, Adv. Mater. 21 (2009) 509–534.
[16] B. Yan, X.F. Qiao, J. Phys. Chem. B 111 (2007) 12362.
[17] B. Yan, X.F. Qiao, Inorg. Chem. 48 (2009) 4714.
[18] V. Bekiari, G. Pistolis, P. Lianos, Chem. Mater. 11 (1999) 3189.
[19] Y.Y. Li, B. Yan, Q.P. Li, Dalton Trans. 42 (2013) 1678.
[20] J. Liu, B. Yan, J. Photochem. Photobiol. A 206 (2009) 32–39.
[21] C. Sanchez, F. Ribot, New J. Chem. 18 (1994) 1007.
[22] B.H. Tong, S.H. Wang, J. Jiao, F.R. Ling, Y.Z. Meng, B. Wang, J. Photochem. Photobiol. A 191 (2007) 74–79.
[23] B. Yan, H. Zhang, S. Wang, J. Ni, J. Photochem. Photobiol. A 112 (1998) 231–238.
[24] Q.M. Wang, B. Yan, Opt. Mater. 29 (2007) 510–515.
[25] A.C. Franville, R. Mahiou, D. Zambon, J.C. Cousseins, Solid State Sci. 3 (2001) 211–222.
[26] N. Xu, W. Shi, D.Z. Liao, S.P. Yan, P. Cheng, Inorg. Chem. 47 (2008) 8748–8756.
[27] J. Miklovic, P. Segl̃a, D. Miklos, J. Titis, R. Herchel, M. Melník, Chem. Pap. 62 (5) (2008) 464–471.
[28] Z. Guo, S. Chen, Q. Yang, S. Gao, Chin. J. Chem. 28 (2010) 383–387.
[29] Y.F. Yue, W. Sun, E.Q. Gao, C.J. Fang, S. Xu, C.H. Yan, Inorg. Chim. Acta 360 (2007) 1466–1473.
[30] M.D. Pechini, U.S. Patent No. 3330697, July 11, 1967.
[31] W. Stöber, A. Fink, E. Bohn, J. Colloidal Interface Sci. 26 (1968) 62–69.
[32] E.R. Leite, A.P. Maciel, I.T. Weber, P.N. Lisboa-Filho, E. Longo, C.O. Paiva-Santos, A.V.C. Andrade, Y. Maniette, W. Schreiner, Adv. Mater. 14 (2002) 905–908.
[33] A.P. Maciel, E.R. Leite, E. Longo, J.A. Varela, Cerâmica 51 (2005) 52–57.
[34] P.C.R. Soares-Santos, H.I.S. Nogueira, J. Rocha, V. Félix, M.G.B. Drew, R.A.S. Ferreira, L.D. Carlos, T. Trindade, Polyhedron 22 (2003) 3529–3539.
[35] S.M.O. Quintal, H.I.S. Nogueira, V. Félix, M.G.B. Drew, Polyhedron 21 (2002) 2783–2791.
[36] G. Socrates, Infrared and Raman Characteristic Groups Frequencies Tables and Charts, third ed., John Wiley & Sons, 2001.
[37] S. Bachmann, L.F.C. Melo, R.B. Silva, T.A. Anazawa, I.C.S.F. Jardim, K.E. Collins, C.H. Collins, K. Albert, Chem. Mater. 13 (2001) 1874.
[38] J.B. Jun, J.K. Hong, J.G. Park, K.D. Suh, Macromol. Chem. Phys. 204 (2003) 2281–2289.
[39] E.J. Nassar, Y. Massaddeq, S.J.L. Ribeiro, Química Nova 25 (1) (2002) 27–31.
[40] E.E.S. Teotonio, M.C.F.C. Felinto, H.F. Brito, O.L. Malta, A.C. Trindade, R. Najar, W. Strek, Inorg. Chem. Acta 357 (2004) 451–460.
[41] I.L.V. Rosa, L.H. Oliveira, C.K. Suzuki, E.R. Leite, J.A. Varela, E. Longo, J. Fluoresc. 18 (2008) 151–155.
[42] I.L.V. Rosa, A.P.A. Marques, M.T.S. Tanaka, D.M.A. Melo, E.R. Leite, E. Longo, J.A. Varela, J. Fluoresc. 18 (2008) 239–245.
[43] T.M. Mazzo, M.L. Moreira, I.M. Pinatti, F.C. Picon, E.R. Leite, I.L.V. Rosa, J.A. Varela, L.A. Perazolli, E. Longo, Opt. Mater. 32 (2010) 990–997.
[44] A.P. Moura, L.H. Oliveira, E.C. Paris, M.S. Li, J. Andrés, J.A. Varela, E. Longo, I.L.V. Rosa, J. Fluoresc. 21 (4) (2011) 1431–1438.
[45] C.A. Kodaira, H.F. Brito, M.C.F.C. Felinto, J. Solid State Chem. 171 (2003) 401.
[46] P.F.S. Pereira, A.P. de Moura, I.C. Nogueira, M.V.S. Lima, E. Longo, P.C. de Sousa Filho, O.A. Serra, E.J. Nassar, I.L.V. Rosa, J. Alloys Comp. 526 (2012) 11–21.